Advances in Aircraft and Spacecraft Science, *Vol. 1*, *No. 3* (*2014*) *353-378*
DOI: http://dx.doi.org/10.12989/aas.2014.1.3.353

On the development of the Anuloid, a disk-shaped VTOL aircraft for urban areas

Marco Petrolo [*1], Erasmo Carrera [1,2a], Michele D'Ottavio [3b], Coen de Visser [4c], Zdeněk Pátek [5d] and Zdenek Janda [6e]

[1] *School of Aerospace*, *Mechanical and Manufacturing Engineering*, *RMIT University*, *PO Box 71*, *Bundoora VIC 3083*, *Australia*
[2] *Department of Mechanical and Aerospace Engineering*, *Politecnico di Torino*, *Corso Duca degli Abruzzi 24*, *Torino*, *Italy*
[3] *Laboratoire Energétique*, *Mécanique et Electromagnétisme* (*LEME*), *Université Paris Ouest*, *50 rue de Sèvres*, *92410 Ville d'Avray*, *France*
[4] *Control and Simulation Division*, *Faculty of Aerospace Engineering*, *Delft University of Technology*, *Delft 2600GB*,*The Netherlands*
[5] *VZLÚ Aerospace Research and Test Establishment*, *Prague*, *Czech Republic*
[6] *6FESA s.r.o.*, *Prague*, *Czech Republic*

(*Received January 14*, *2014*, *Revised March 22*, *2014*, *Accepted April 28*, *2014*)

Abstract. This paper deals with the early development of the Anuloid, an innovative disk-shaped VTOL aircraft. The Anuloid concept is based on the following three main features: the use of a ducted fan powered by a turboshaft for the lift production to take-off and fly; the Coanda effect that is developed through the circular internal duct and the bottom portion of the aircraft to provide further lift and control capabilities; the adoption of a system of ducted fixed and swiveling radial and circumferential vanes for the anti-torque mechanism and the flight control. The early studies have been focused on the CFD analysis of the Coanda effect and of the control vanes; the flyability analysis of the aircraft in terms of static performances and static and dynamic stability; the preliminary structural design of the aircraft. The results show that the Coanda effect is stable in most of the flight phases, vertical flight has satisfactory flyability qualities, whereas horizontal flight shows dynamic instability, requiring the development of an automatic control system.

Keywords: VTOL; Coanda effect; aircraft design; flyability analysis; CFD

1. Introduction

The capability of an aircraft to take-off and land vertically or in limited spaces avoids the need for classical airport installations and dedicated runways and promotes excellent mission versatility.

∗Corresponding author, Research Fellow, E-mail: marco.petrolo@rmit.edu.au
[a] Professor, E-mail: erasmo.carrera@polito.it
[b] Professor, E-mail: michele.d_ottavio@u-paris10.fr
[c] Assistant Professor, E-mail: C.C.deVisser@TUDelft.nl
[d] Researcher, E-mail: patek@vzlu.cz
[e] Researcher, E-mail: zdenek.janda@centrum.cz

http://www.techno-press.org/?journal=aas&subpage=7 ISSN: 2287-528X (Print), 2287-5271 (Online)

The development of VTOL (Vertical Take-Off and Landing) machines has therefore continuously attracted aeronautical engineers. The design of VTOLs must consider some specific issues, amongst them, the most important are the following (Lindenbaum 1986):

- Hover and forward flight (cruise) efficiency.
- Transition behavior and flight control quality.
- Environment condition: downwash velocity and temperature, noise.

According to the variety of design criteria, a large number of very different VTOL concepts have been considered in the history of aeronautics. A brief overview of the main VTOL categories is provided hereafter.

Helicopters are the most successful VTOL aircraft for both civil and military applications. Helicopters can land and take-off in unprepared and difficult to access areas (e.g., mountains and deserts) and in small, dedicated helipads. These features make helicopter the privileged aerial transportation vehicle for emergency operations in urban areas, offshore platforms or large boats. Another key advantage of helicopters is their efficiency in hover. The large rotor promotes a low disc loading (i.e., the ratio between the produced thrust and the surface of the rotor), which in turn minimizes the required power for lift generation (Stepniewski and Keys 1984). On the other hand, helicopters have low forward flight speeds and limited cruise efficiency. Furthermore, the main rotor is a very complex system because it has to accommodate both vertical and horizontal flight conditions (Johnson 2004). The long blades undergo highly variable aerodynamic loads and severe dynamic loadings (e.g., centrifugal forces and the vibrations that are induced by the aerodynamic pressure variations). Moreover, the exposed, long rotating blades of the main rotor restricts the accessible areas of helicopters for safety reasons and the noise pollution regulations restrict the allowable noise and, therefore, prevent helicopters to access a large number of urban and sub-urban areas. It is also important to emphasize that the unprotected rotor noticeably reduces the weather-conditioned clearances of helicopters. A typical example is the icing problem (Gent 2010), where ice accretion on the rotating, unprotected blades can substantially modify the airfoil, thus dramatically reducing the lifting capability of the rotor and increasing the drag.

A number of VTOL aircraft have been developed in the last decades whose cruise speeds and efficiencies are comparable to those of conventional airplanes. The propulsion system can be considered as the discriminating and most critical aspect of these VTOLs. According to Nelms and Anderson (1984), the propulsion system often represents one of the main reasons for the impracticability of a VTOL. The propulsion system can affect, in fact, the handling qualities, in particular during transition from vertical to horizontal flight and vice versa. It is emphasized that in a VTOL, the flight control quality is intrinsically associated to the propulsion system. In fact, while conventional airplanes are controlled through effective aerodynamic surfaces, in a VTOL the required control forces in sub-aerodynamic flight regimes (e.g., vertical hover) have to be in general provided by the propulsion system (Curtis 2010). A first VTOL classification can be carried out with respect to the power/lift distribution (Lindenbaum 1986):

- Wingless aircraft whose lift generation relies entirely on the thrust generated by the propulsive system.
- Winged aircraft in which the required lift is power-generated only in the sub-aerodynamic regime while it is aerodynamically generated once a sufficient cruise speed is reached.

A more detailed VTOL classification is based on the propulsion systems that are employed for the generation of the lifting force and for the cruise (Lindenbaum 1986):

- Two separated engine sets for lift and cruise ($L + C$ configuration).

- A primary *L*/*C* engine set and a lift generating engine set (*L*/*C* + *L* configuration).
- A primary *L*/*C* engine set with thrust augmentation for VTOL (*L*/*C* + *A* configuration).
- Only one engine set generating both lift and cruise (*L*/*C* configuration).

These four configurations are detailed out hereafter.

The *L* + *C* configuration is based on the idea of implementing two separated propulsion systems for lift and cruise (*L* + *C*) to simplify the engine installation and to use the different engine sets only for the function they are designed for to optimize their efficiency. The main drawback stems from the large number of engines required for lift that dramatically reduces the useful payload. Two French aircraft were designed according to this configuration by Dassault Aviation in the mid-1960s, the Mirage III V and the Balzac V (Hirschberg *et al*. 2002). The initial concept of the military cargo aircraft Fiat G-222 (first flight in 1970) was equipped with two turboprop engines for cruise and several turbojet engines for lift generation (Hirschberg *et al*. 2003). The VTOL capability has been subsequently discarded from this aircraft to improve the payload as well as operational range and the G-222 turned out to be a reliable Short Take-Off and Landing aircraft (STOL). The advantages in terms of payload and flyability obtained upon converting VTOL into STOL capabilities have been documented for different concepts (Deckert 1995).

In the *L*/*C* + *L* configuration, an additional engine set that is purely dedicated to the lift generation assists the primary *L*/*C* engine set. A successful example has been the Russian transonic fighter Yakovlev Yak-38 (first flight in 1971).

The *L*/*C* + *A* configuration implements an augmented thrust generator that is driven by the primary *L*/*C* engine set. Two different categories can be identified, in the first one the thrust augmentation is used to enhance the cruise flight whereas in the second one is used to produce the required lift. Compound helicopters with short wings belong to the first category. In these aircraft, the engine drives an additional rotor to increase the cruise speed. This means that the standard helicopter configuration is used during hover while, for forward flight, the engine power is redirected to the additional (horizontal) thrust generator while the wings contribute to generate the required lift. The Piasecki 16H-1 Pathfinder (first flight 1962, civil applications) and the Lockheed AH-56 Cheyenne (1967, military use) are two examples of this category. The most important example for the second category is the recently developed F-35B Joint Strike Fighter. This airplane is equipped with a dedicated turbofan engine whose by-pass flow can be used during hover to drive a lifting fan embedded into the front part of the fuselage (Curtis 2010).

The embedding of a propeller into the aircraft structure (fuselage or wing) leads to the creation of a ducted fan which enhances the generated thrust with respect to the un-shrouded propellers of the same size. This enhancement is due to the reduction of the tip loss and to the optimization of the airflow velocity and pressure through an accurate duct design (Fite 2013). Moreover, the duct can host passive or active acoustic dampers for reducing the noise of the engine. A number of models that are based on this solution have been recently developed by the Israeli company UrbanAero (Urban Aero) in cooperation with the Bell Helicopters (e.g., the AirMule, the Centaur and the X-Hawk). The airframe of these aircraft only marginally provides aerodynamic lift, the ducted fans actually operate as powered lift generators for these wingless configurations. All ducted fans are driven by the same engine, which on one hand reduces the propulsion system weight but on the other hand requires the use of power transmission mechanisms requiring adequate maintenance.

The *L*/*C* minimizes the number of thrust-generating devices at the price of an adequate system to vector the thrust between the horizontal (cruise flight) and vertical (hover) direction. Many different implementations of this concept have been proposed, the differences consist in the ways

the thrust is generated and vectored. In the deflected slipstream configuration, the trailing edge flaps deflect the propeller slipstream. The Ryan 92 (first flight in 1959) was a full-metal aircraft and proved to be too heavy to lift without an important head wind. In general, this concept suffers important ground effects that reduce the hovering performances, in particular due to the slipstream recirculation and requires particular pilot skills to control the transition phase and the flight regimes at low power (e.g., steep descent approaches) (Nelms and Anderson 1984).

In the tilt wing configuration, the wing carries the engine nacelle and is tilted. A representative example was the LTV-Hiller-Ryan XC-142 cargo aircraft (first flight in 1964). In vertical flight, the wings are in the airflow of the propellers, this reduces the lift-opposing download generated by the propeller downwash on the wings and allows the ailerons to control the yaw motion. However, variable propeller slipstream circulations due to ground effect, longitudinal stability and low directional control power were unresolved issues of this concept. Moreover, an uncontrolled "balloon" trajectory occurs during transition to hovering flight due to the angle of attack increase of the tilting wing (Knowles 2010).

In the tilt shaft configuration, the wing and the nacelle are fixed, only the propeller/rotor shaft is tilted. The Bell XV-3 (first flight in 1955) has served as basis for the subsequent tilt rotor developments (Bell XV-15) despite suffering important dynamic instability of the rotors that caused extremely high cockpit vibrations. The tilt prop/duct/rotor has the nacelle carrying the rotor, the propeller or the ducted fan tilted and the wing is kept fix. The Curtiss-Wright X-19 (first flight in 1963) has four tilting propellers (two on wings and two on tail) driven by two turboshaft engines located in the fuselage. This concept suffered an excessively complex and sensitive mechanics and was early cancelled due to a crash procured by a transmission part failure. The Bell X-22 (first flight in 1966) had 4 tilting ducted fans and served as basis for the development of a variable stability and control system. Afterwards, the Bell XV-15, the Bell-Boeing V-22 and the Agusta-Westland AW609 were developed (Maisel *et al*. 2000). With respect to the tilt wing design, the tilt rotor has a broader transition corridor but loses efficiency in vertical lift due to download effect (Knowles 2010). The military aircraft Bell-Boeing V-22 (first flight in 1989) is nowadays produced for the US Navy, Air Force and Marine Corps and has proven its excellent tactical features in several combat scenarios. Special noise certifications were required for tilt rotor aircraft (Federal Aviation Administration 2013). Both the V-22 and the AW609 make extensive use of composites for the weight reduction and the aeroelastic tailoring and are equipped with redundant fly-by-wire control systems with stability enhancement for ensuring the necessary handling qualities, in particular during transition (Landis *et al*. 1994, Bianco-Mengotti 2012). In contrast to the V-22, the AW609 has a pressurized cabin that improves passengers' comfort. Moreover, both models can operate as STOL aircraft, which permits to increase their payload.

In the tilt outer wing with rotor configuration, the outer wing portion tilts along with the engine nacelle; it is thus a combination of tilt wing and tilt rotor configurations. This concept, known as ERICA (Enhanced Rotorcraft Innovative Achievement), is being analyzed since 2000 within a continuing European Tilt-rotor program. The key advantages of this concept are: (1) to improve hover efficiency by reducing the rotor download on the wing in helicopter mode; (2) to reduce the complexity of the tilting mechanism by rotating a single mass through a torque tube inside the wing (Bianco-Mengotti 2012).

The *L*/*C* configurations that have been reviewed so far, have prop or rotor thrust. A number of *L*/*C*s that are based on jet thrust were developed. In a tilt jet, the turbojet engines are fixed under the wing and tilted. The Bell 65 Air Test Vehicle (first flight in 1954) has been the only aircraft developed with this configuration. Another option is the vectored thrust in which the exhausts of a

jet engine are oriented through movable nozzles. The transonic ground-attack Hawker-Siddeley AV-8 Harrier (first flight in 1969) has been the first VTOL aircraft produced in series.

Tail sitters are aircraft in which the longitudinal axis is positioned vertically at take-off, the thrust is always kept parallel to the longitudinal axis. The Ryan X-13 (first flight in 1955) is a representative successful example of this configuration.

The turbojet airflow can be ducted; this means that the vertical and the horizontal thrust are realized by a controlled airflow generated by ducting fan and engine exhaust. The control of the airflow can be realized by movable vanes exploiting the so-called Coanda effect, which can be described as follows: "a stream of air at high velocity will attach to a curved surface rather than follow a straight line in its original direction" (Barlow *et al*. 2009). The lift production through a ducted airflow was the basic idea of the very unusual "flying saucer" VTOL aircraft developed in the 1950s by the Canadian company Avro and the US Air Force, the VZ-9AV "Avrocar" (Lindenbaum and Blake). It was conceived as an annular wing obtained upon rotating an airfoil about its leading edge, which hosted three turbojet engines driving a central rotor whose aspired air was mixed to the exhaust gases and ducted to a peripheral annular nozzle. This ducted flow followed the nozzle geometry (by exploiting the Coanda effect) and was oriented underneath the Avrocar, thus promoting lift. Unfortunately, the only produced effect was a favorable ground effect that permitted the Avrocar only to float at a very moderate height (approximately 1 m). Additionally, uncontrolled pitch instability affected the forward flight at moderate speed and the cockpit resulted to be excessively noisy and hot. The inclusion of too many novelties in the Avrocar has been identified as the reason for the concept failure, several innovative and thus not yet fully demonstrated technologies were used to control the aircraft, e.g., pneumatically powered flight control systems or the gyroscopically stabilized rotor. The ducted airflow and Coanda effect have recently found increased application in VTOL unmanned aerial vehicles (UAV) (Crivoi *et al*. 2013).

From these studies, it appears that two synergic lifting mechanisms can be activated by the Coanda effect by ducting the airflow at high velocity over a curved surface:

- The curved surface can redirect the airflow downwards, this leads to the production of vertical thrust.
- The deflected airflow can entrain surrounding air, inducing a low-pressure region above the body and thus lift.

The first way of producing lift has been demonstrated to be largely dominant over the second

(a) 3D view (b) Cross-sectional view

Fig. 1 Anuloid geometry

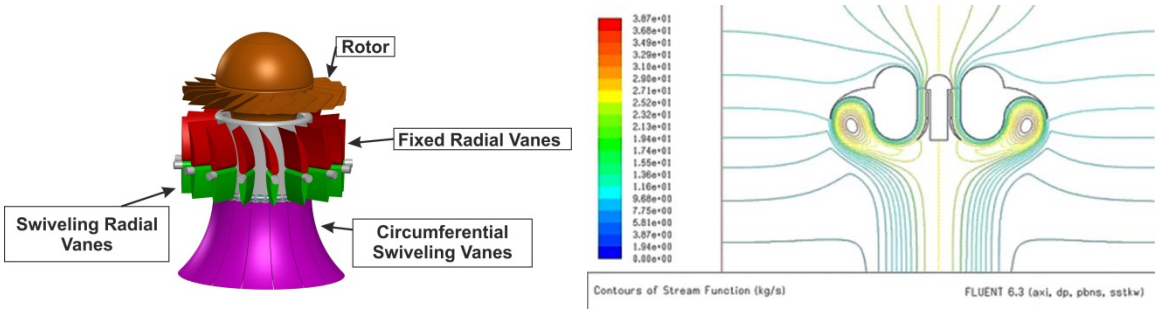

(a) Turboshaft, anti-toque and control blades (b) Coanda's effect

Fig. 2 Anuloid main characteristics

one. Moreover, the deflection of the downstream should permit to control pitch, roll and yaw. It is also interesting to report research activities aimed at reducing rotor downwash on tilt rotor aircraft by means of the Coanda effect (Angle *et al*. 2006).

The present paper presents the early development of a disk-shaped VTOL aircraft hereafter referred to as the Anuloid (Janda 2009). This aircraft is an *L*/*C* in which the ducted airflow from a fan powered by a turboshaft contributes to the lift generation together with the Coanda effect that is also exploited for the flight control. This paper is organized as follows: the Anuloid is briefly described in Section 2, the preliminary structural design is presented in Section 3, CFD analyses are shown in Section 4, the flyability analysis is outlined in Section 5 and the main conclusions are drawn in Section 6.

2. Anuloid at a glance

The Anuloid is a VTOL aircraft with a toroidal shape and a turboshaft engine in its center that drives a ducted rotor (Fig. 1). The outer diameter is equal to 5 m, the maximum take-off weight should not exceed 1200 kg. Only one propulsion system is implemented for both lift and cruise (*L*/*C* configuration), this should lead to a more favorable payload-to-empty weight ratio. The forward flight speed of the Anuloid is expected to be in the 100-200 km/h range. The typical operating scenarios are the emergency missions and civil transportation in urban areas. Fig. 2(a) shows the rotor configuration and the system of fixed and movable blades that is placed in the inner vane of the aircraft. Fig. 2(b) shows a preliminary CFD analysis that highlights the Coanda effect. The accelerated flow goes through the fixed and the swiveling radial vanes that, by controlling the swirl of the flow, eliminate the rotor torque and provide yaw control. The circumferential swiveling vanes duct the airflow to the bottom, curved surface of the aircraft. Through the Coanda effect, the flow remains attached to this surface and finally accelerates downwards through the large section defined by the outer diameter of the aircraft. The individual swiveling of the circumferential vanes can control the tilting of the aircraft by local variations of the resistance to the airflow. The Anuloid can head towards the tilting direction. Control forces and moments for the Anuloid are obtained through the manipulation of the ducted airflow and the Coanda effect. This aircraft belongs to the wingless configurations since lift is essentially power

generated, the circular fuselage being supposed to produce only marginal additional lift during cruise.

This paper presents the structural, aerodynamic and flight mechanic preliminary analyses of the Anuloid. The aim of these analyses is the investigation of the feasibility and the flyability of this concept.

3. Weight estimation and preliminary structural design

A CAD model of the Anuloid was first built to estimate the mass properties of the aircraft. The mass estimation that was obtained from the CAD model is reported in Table 1.

A preliminary structural design of the aircraft was carried out. The main aims of this preliminary design activity were the following:

- The creation of the preliminary structural layout of the aircraft.
- In particular, the main structural frame of the aircraft was considered.
- The secondary structural components were not considered.

Table 1 Mass estimation from the design specifications and the CAD model

Component	Mass (kg)
Structure	215
Engine	247
Undercarriage	35
Fuel	217
Systems	90
Payload	380
Total	**1184**

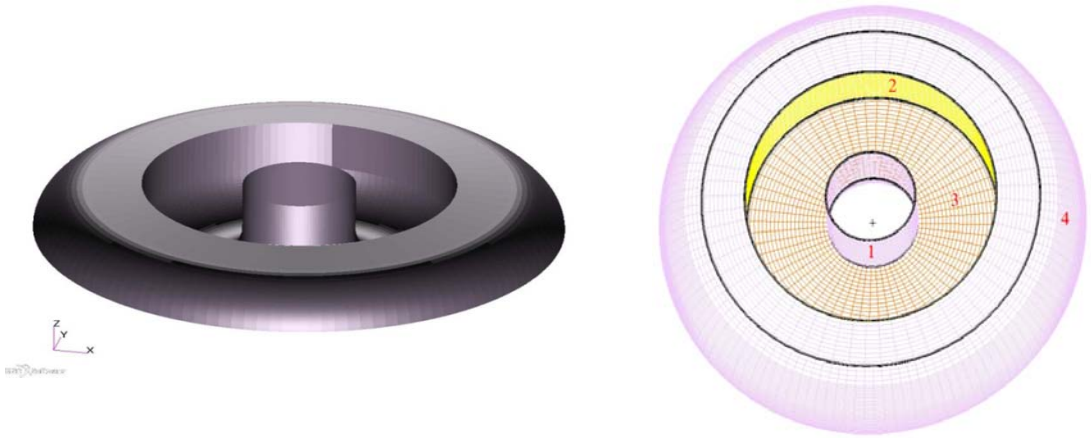

(a) Fuselage (b) Material distribution

Fig. 3 Structural model of the fuselage

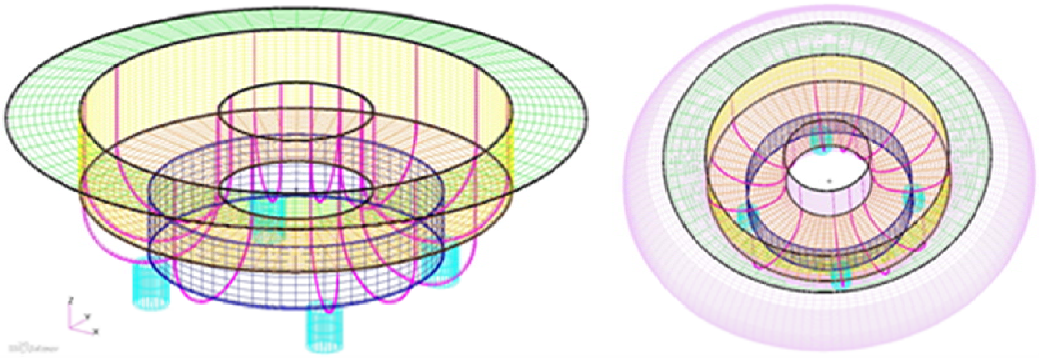

Fig. 4 Main structural frame of the Anuloid

The structural model was built in MSC Patran and is shown in Fig. 3. A possible material distribution within the fuselage was also proposed as shown in Fig. 3(b), parts 1-2 will be assumed made of Carbon Fiber Reinforced Polymer (CFRP), whereas parts 3-4 will be assumed made of sandwich panels.

Fig. 4 shows the preliminary design of the main structural frame of the Anuloid, the main components are

- 2D panels made of composite materials.
- A frame of stiffeners (bolded lines). These stiffeners are required to bear a number of loads, such as those due to the engine or the landing legs.
- The landing legs that were assumed cylindrical.

A linear static analysis was carried out in MSC Nastran by considering the following loads: payload weight, fuel weight and the engine weight. Fig. 5 shows the maximum failure index

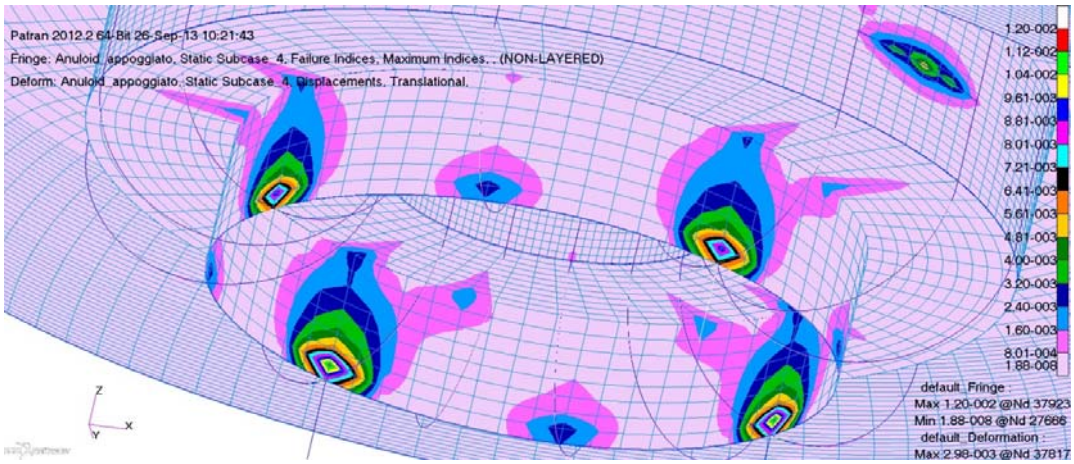

Fig. 5 Failure index distribution around the landing legs

values (about 0.01) that were found around the landing leg connection points. This failure index value is extremely low, however a further optimization of the structure will be carried out by considering the other load sets (e.g., maneuver loads and aerodynamic loads). According to the material densities and assuming typical values of thicknesses, the weight of the entire structural model can be equal to about 160 kg.

The structural design of the Anuloid should not be critical since a relative light structure can be designed with no particular structural issues. Particular attention should be paid to the design of the wing to avoid aeroelastic issues.

4. Aerodynamic analysis

The aerodynamic analysis was carried out by means of CFD tools and it was divided into two parts, the analysis of the vertical and of the horizontal flight. The main aims of the analyses were the investigation of the Coanda effect, the computation of the aerodynamic data for the flyability analysis and the investigation of some design parameters (e.g., rotor diameter, angle of the control vanes, etc.).

4.1 Vertical flight

The software that was used for the CFD analysis of the vertical flight was Ansys Fluent 14.5, whereas JMP and Design Expert were exploited for the design of experiments and for the response surface method. On the basis of the CAD model of the Anuloid, the following assumptions were used to determine whether the lift force that is achievable during the vertical flight is sufficient:

- The Anuloid CAD-computed total weight is 1184 kg.
- The take-off power was set equal to 1,34 MW by assuming the Honeywell T5317BCV as engine.

The CFD analysis was carried out according to the following parameter setup:

- Periodic boundary conditions were used and the rotor was substituted by an annular disc with a prescribed volume flow.
- The Reynold Stress Model (RSM) was exploited for the turbulence modeling.
- The steady state method was used.
- Six input parameters (or factors) were used.
- Five primary outputs were evaluated.
- 56 CFD analysis cases were considered.

Table 2 shows the inputs and their ranges that were used for the analysis. These parameters were then normalized (-1; 1) to obtain the normalized response surface functions whose coefficients show the relative significance of the different parameters and of their combinations.

Fig. 6 shows the pathlines for the following combination of inputs: rotor diameter = 1.1 m, length of the radial control vane = 0.3 m, angle of the radial control vane = 10 deg, 16 radial control vanes, volume flow = 100 m^3/s and vertical velocity = 0 m/s. This combination was chosen since it is representative of the flow during hover. The surface of the Anuloid is not shown for the sake of clearness. Fig. 6 clearly shows that the outer pathlines of the flow generated by the rotor create an annular vortex located below the bottom surface of the outer part of the Anuloid, which, as the CFD analysis proved, is stable for all the computed cases. This is very important because it ensures

Table 2 Inputs for the CFD analysis of the vertical flight

Parameter	Range	Unit
Rotor diameter	1.0 – 1.2	m
Number of the radial control vanes	8 – 16	–
Length of the radial control vanes	0.2 – 0.3	m
Angle of the radial control vanes	0 – 10	deg
Volume flow through the rotor	80 – 100	m^3/s
Vertical velocity	-5 – +5	m/s

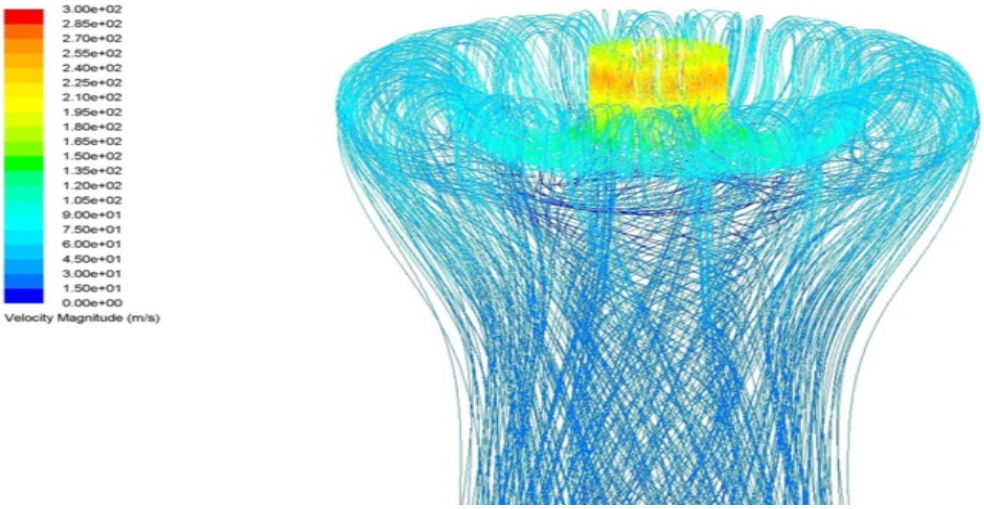

Fig. 6 Outward pathlines from the rotor colored by velocity magnitude

the stability of the vertical flight. Since the angle of the radial control vanes is nonzero in the presented case, there is also strong whirling around the axis of symmetry of the Anuloid, which should cause, by reaction, the controlled yaw motion.

The response surface functions for the axial moment, the lift force and the required power were derived from the results of the 56 CFD analysis cases with carefully designed different combinations of input parameters. These functions provide analytical expressions of the dependency of the Anuloid vertical flight properties on the input parameters. The properties of these functions can be easily visualized and their main utilization is in the flight dynamics and the flight performance analyses. Fig. 7 shows a response surface example in which it can be seen how for each value of the volume flow the required power is very weakly dependent on the vertical velocity.

The main results that were obtained through the CFD analysis of the vertical flight are the following:

(1) The Coanda effect is stable for all the combinations of the geometrical and the physical parameters.
(2) The achievable yaw control moment is good.

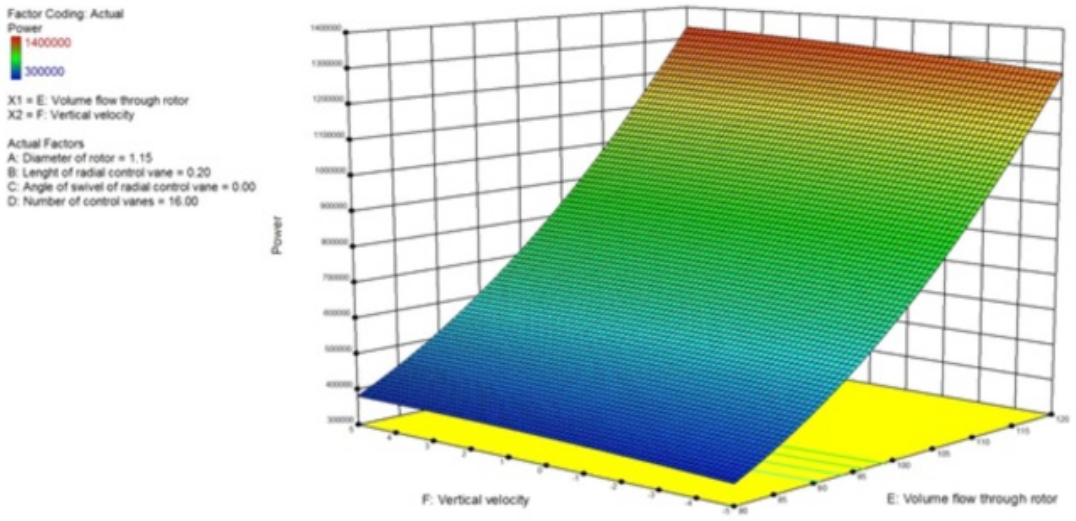

Fig. 7 Required power dependency vs the volume flow through the rotor and vs the vertical velocity

(3) The achievable lift force for the Anuloid aircraft in relation to the power of the considered engine is sufficient for the vertical flight in the range of the investigated vertical velocities (-5 m/s , +5 m/s) with the rotor diameter at least equal to 1.15 m.

4.2 Horizontal flight

The CFD analysis of the horizontal flight was carried out by replacing the set of individual separated control vanes with a continuous smoothly deformable collar without distinguished individual vanes. The RANS equations were solved in EDGE, a FOI's in-house computational fluid dynamic (CFD) program package. EDGE is a finite volume Navier-Stokes solver for unstructured meshes. A hexahedral grid was generated in ANSYS ICEM CFD. The boundary layer was simulated by O-grid. The total number of elements was about 3 million. The height of the first layer was adequately small to satisfy the requirements of the turbulence model on the wall function $y+$ in all cases.

The CFD analysis of the horizontal flight was carried out for the following main reasons:

- To verify the development and the stability of the Coanda effect.
- To calculate the aerodynamic force and moment coefficients.
- To verify the effectiveness of the circumferential control vanes of creating sufficient control moment.

Thirty flight conditions were considered. The following four variable parameters were considered:

(1) The position of the circumferential control vanes, in particular, three positions were studied.

(2) Three flight speeds were considered, +1, +30, -30 m/s. The positive flight speed indicates forward flight, the negative flight speed indicates backward flight. This difference is

important due to the geometric asymmetries caused by the asymmetric deflections of the circumferential control vanes.

(3) The mass flow through the fan of the power unit was set equal to 80, 90, 100 m^3/s. The rotor diameter was set equal to 1.20 m.

(4) Three angles of attack were considered, 0, +10, and -10 degrees.

The cross-section of the internal duct between the main Anuloid body and the downstream body of the power unit was designed with a constant width of the gap between the body and the rear part of the power unit body (Fig. 8). This geometric design caused the increase of the duct cross-section area in the downstream direction.

The CFD analysis of the initial configuration has shown that there were flight regimes without a stable Coanda effect below the Anuloid body. An example of such a regime is presented in Fig. 9. The problem was analyzed and the probable source of the instability was found in the geometry of the duct between the Anuloid main body and the rear (lower) part of the power unit body. The

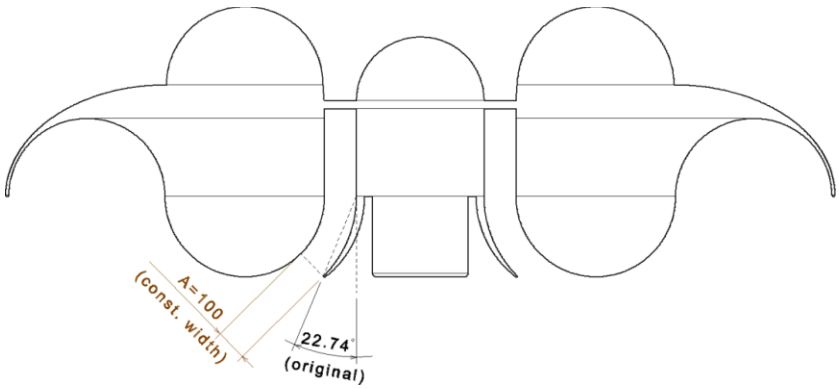

Fig. 8 Initial baseline deflection of the circumferential control vanes

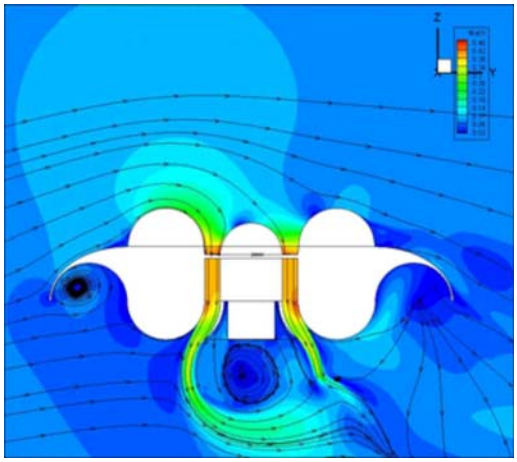

Fig. 9 Streamline and Mach distribution around the initial configuration, flight speed = 1 m/s, mass flow = 80 m^3/s and angle of attack = -10°

proposed remedy consisted in the modification of the geometry of the internal duct; it was found that the change of the constant cross-section of the duct is sufficient. This requirement was met by a simple change of the baseline deflection of the circumferential control vanes.

The basic symmetric angular deflection of the circumferential vanes was increased from 22.74° to 29.25° (V10 deflection designation, Fig. 10(a)). The cross-section of the internal duct between the main Anuloid body and the rear (lower) body of the power unit was changed in order to keep the cross-section area constant moving downstream in the duct. Two asymmetric deflections of the circumferential control vanes were studied. In both cases, the vanes on one half of the Anuloid were in the basic position (29.25°). The deflections of the collar of vanes of the second half were smoothly linearly extended from the basic position to have the vane at the extreme outer position maximally deflected (Fig. 10(d)). In the half asymmetric deflection (V8 deflection designation, Fig. 10(b)) the half of the vanes were in the basic position (29.25°). The deflections of the collar of vanes of the second half were smoothly linearly developed from 29.25° to 33.32°. In the fully asymmetric deflection (V6 deflection designation, Fig. 10(c)) , half of the vanes were in the basic position (29.25°). The deflections of the collar of vanes of the second half were smoothly linearly developed from 29.25° to 37.15°.

Table 3 presents the combinations of the parameters that were considered for the analyses. For the sake of brevity, only ten cases have been reported. Tables 4 and 5 present the forces and moments and their coefficients for the considered cases without the influence of the power thrust and with the influence of the thrust, respectively. By considering the supposed mass of the aircraft (approximately 1000–1100 kg) , the Anuloid is able to generate sufficient lift for a good number of combinations. The circumferential vanes create pitching and rolling control moments in a satisfactory range.

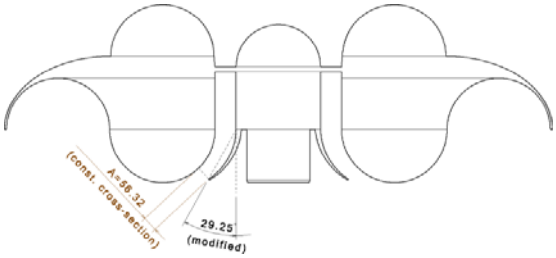

(a) Symmetric angular deflection, V10

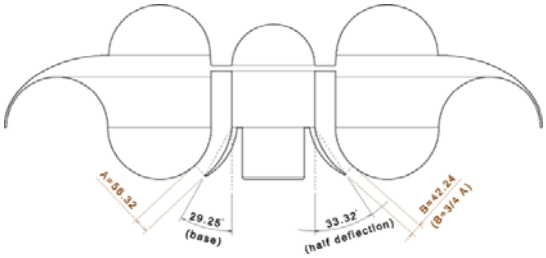

(b) Half asymmetric deflection, V8

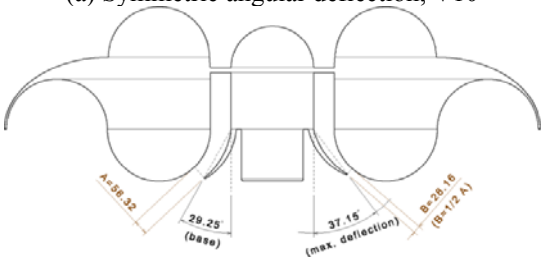

(c) Fully asymmetric deflection

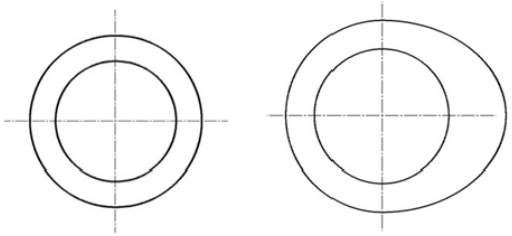

(d) Horizontal plan of symmetric and asymmetric deflection of the "collar" of the circumferential control vanes

Fig. 10 Final baseline deflection of the circumferential control vanes

Table 3 Combinations of the vane deflections, flight speeds, mass flows and angles of attack

Case	Vane deflection	Flight speed (m/s)	Mass flow (m^3/s)	Angle of attack (deg)
1	V6	-30	100	-10
2	V10	30	100	10
3	V10	30	100	-10
4	V6	-30	80	-10
5	V10	-30	80	0
6	V10	-30	80	10
7	V6	30	100	-10
8	V6	1	90	-10
9	V10	-30	100	-10
10	V10	-30	100	10

Table 4 Aerodynamic forces without the influence of thrust

Case	F_L (N)	F_D (N)	M (N·m)	C_L	C_D	C_M
1	951,79	2551,95	-782,89	0,162601	0,43597	-0,02572
2	8391,11	4102,33	-2737,61	1,433522	0,700835	-0,08994
3	2588,23	2402,65	-2492,29	0,442168	0,410464	-0,08188
4	982,30	2368,42	318,66	0,167814	0,404616	0,010469
5	4047,05	2262,01	1903,29	0,691391	0,386438	0,06253
6	7520,58	3494,30	1512,35	1,284803	0,596959	0,049686
7	4422,20	2776,12	-7852,79	0,755481	0,474266	-0,25799
8	-52,87	370,50	-4882,44	-8,12955	56,9654	-144,365
9	2723,39	2341,29	3011,00	0,465259	0,399981	0,098922
10	8424,92	4193,11	2147,09	1,439298	0,716344	0,070539

Table 5 Aerodynamic forces influenced by thrust

Case	F_L (N)	F_D (N)	M (N·m)	C_L	C_D	C_M	T (N)
1	7274,42	1437,10	-782,89	1,242749	0,245511	-0,02572	6420,17
2	15020,04	5271,19	-2737,61	2,565995	0,900521	-0,08994	6731,18
3	9222,57	1232,83	-2492,29	1,575568	0,210615	-0,08188	6736,69
4	4410,51	1763,93	318,66	0,753484	0,301347	0,010469	3481,10
5	8000,65	2262,01	1903,29	1,366816	0,386438	0,06253	3953,59
6	11400,07	4178,35	1512,35	1,947567	0,713822	0,049686	3939,33
7	10647,80	1678,38	-7852,79	1,81905	0,286731	-0,25799	6321,63
8	4785,39	-482,62	-4882,44	735,7747	-74,205	-144,365	4912,90
9	9307,35	1180,36	3011,00	1,59005	0,20165	0,098922	6685,52
10	15064,67	5363,88	2147,09	2,57362	0,916355	0,070539	6742,17

The streamlines Mach number and pressure distributions for the first four cases are shown in Fig. 11; pressures are expressed in Pascal (Pa). These figures show that the Coanda effect was developed on the bottom side of the Anuloid body in all computed cases. The principal aerodynamic feature of the Anuloid – the creation of a stable Coanda effect – was achieved for all

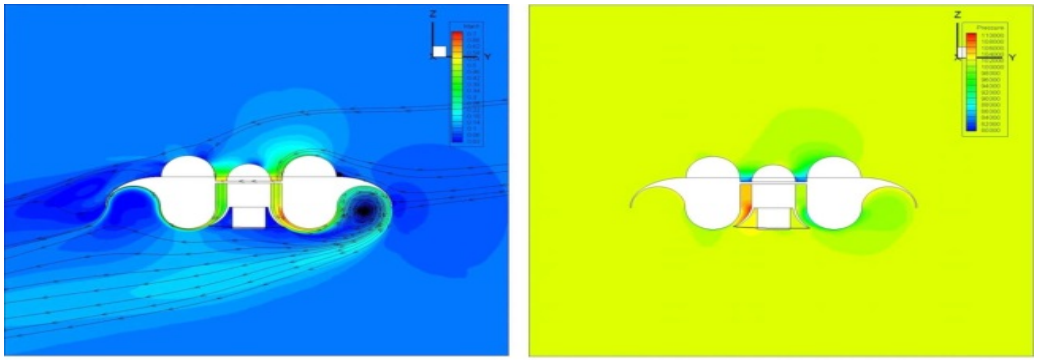

(a) Case 1

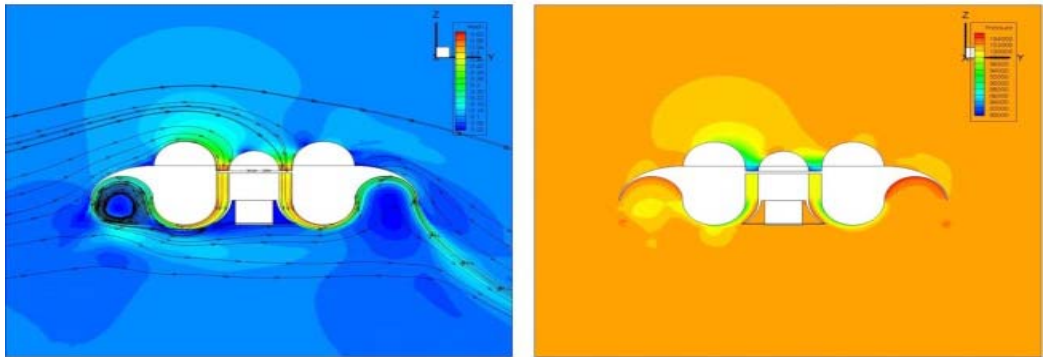

(b) Case 2

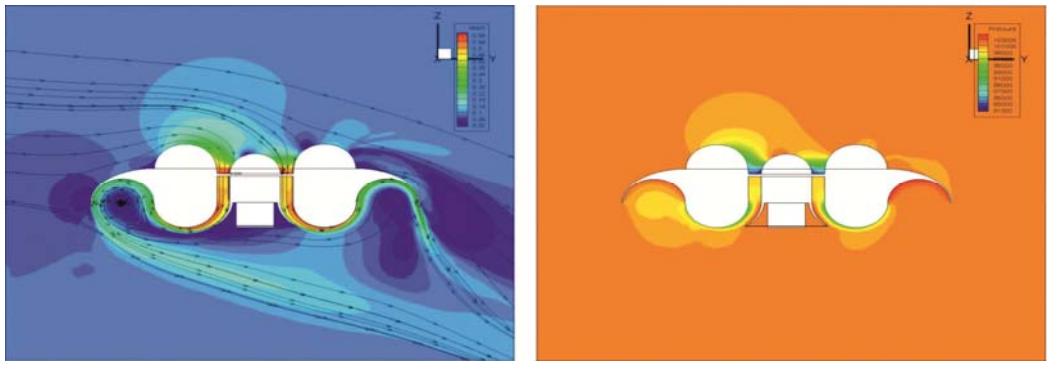

(c) Case 3

Fig. 11 Streamline, Mach and pressure distributions for different configuration of the Anuloid

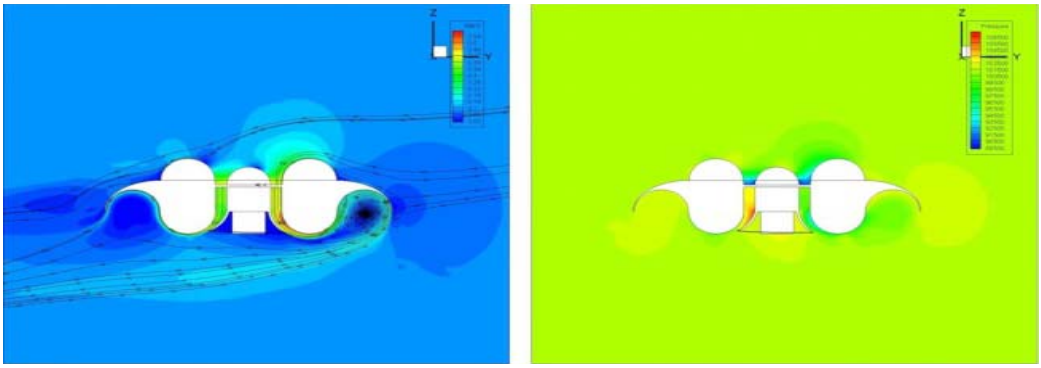

(d) Case 4

Fig. 11 Continued

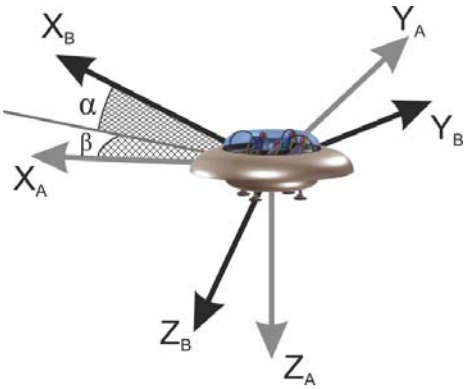

Fig. 12 Reference frame for the flyability analysis

computed angles of attack, flight speeds, mass flows through the fan and circumferential vane deflections. The maximum Mach number in the flow was in the order of 0.65, it seems to be sufficiently below the strong compressibility effect region.

The main results of the CFD analyses of the horizontal flight are the following:

(1) A stable Coanda effect was developed in all the studied static cases after a geometric modification of the internal duct, i.e., after adjusting the basic position of the circumferential vanes.
(2) The aircraft is able to generate sufficient lift in horizontal flight in many flight configurations.
(3) The circumferential control vanes are able to create control moments in pitch and roll.

5. Flyability analysis

The flyability analysis of the Anuloid is presented hereafter, where flyability is defined as the combination of the static performance, together with a static and dynamic stability analysis. Fig.

12 shows the reference frame that was adopted for the flyability analysis. A rotor diameter of 1.3 m was used, together with 16 radial control vanes of length 0.3 m. A diameter of 1.3 meter was used in the analysis, as this resulted in the highest excess power numbers, and thus the highest overall performance. This is a small extrapolation (< 10%) of the maximum value used in the CFD calculations, which is within the specified extrapolation bounds.

5.1 Static performance analysis

The static performance analysis was carried out to investigate the Anuloid capabilities in terms of lift production to take off, perform horizontal flight and land given the maximum power produced by the power plant. The static performance analysis was focused on the analysis of lift and drag curves as a function of the angle of attack and velocity. This analysis uses the immediate responses given an initial flight condition obtained from CFD for aerodynamic lift, drag and moments.

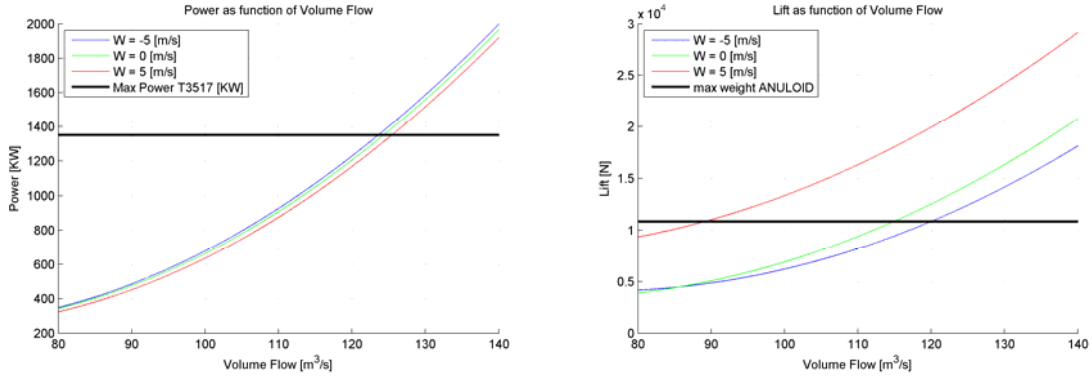

(a) Power (b) Lift

Fig. 13 Power and lift vs mass flow

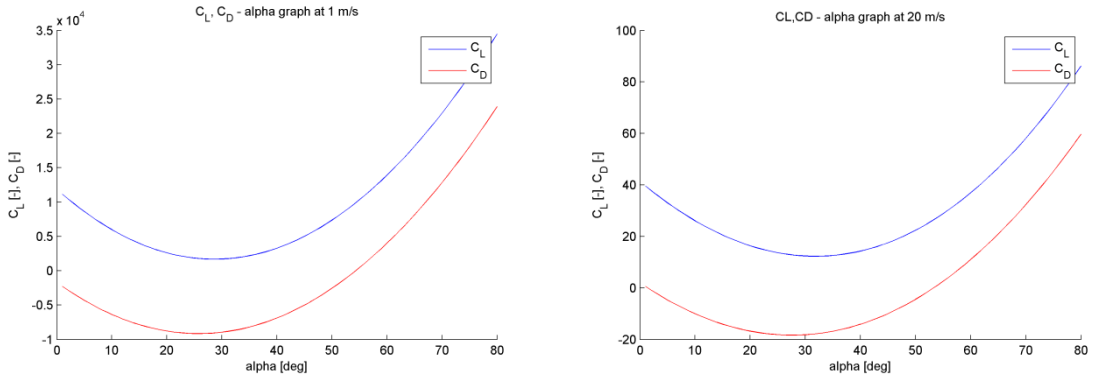

(a) 1 m/s (b) 20 m/s

Fig. 14 C_L/C_D as a function of the angle of attack for different horizontal velocities

Fig. 13(a) shows the static analysis of the required power for a given vertical velocity as a function of the rotor volume flow. Note that W is defined along the positive *Z*-axis in the body reference frame, (i.e., $W < 0$ is ascending flight). Clearly, the maximum output from the Honeywell T3517 (1.35 MW) is sufficient to sustain a maximum mass flow of 125 m^3/s at any vertical velocity between -5 m/s and +5 m/s. Fig. 13(b) shows the lift for a given vertical velocity as a function of the volume flow. The black line is the maximum takeoff weight of the Anuloid (1105 kg). It can be seen that at 120 m^3/s and W = -5 m/s (ascending flight) a sufficient lift is produced to support the weight of Anuloid.

The C_L/C_D graphs were then evaluated (see Fig. 14). The Anuloid has a very wide flight envelope in terms of angle of attack, this means that the graphs cannot be compared directly to similar graphs for conventional aircraft. Despite this, the graphs provide important information on the static performance during the horizontal flight.

5.2 Static stability analysis

The static stability analysis was focused on the analysis of the static moment equilibrium at different angles of attack. In particular, when the pitching moment increases as the angle of attack increases, the aircraft is considered statically unstable, and vice versa. This analysis used directly the response surfaces obtained from CFD for the aerodynamic lift, drag and moments. The static stability analysis was conducted over the angel of attack (AoA) range from 0 to 80 degrees and at horizontal velocities of 1 m/s and 20 m/s. Fig. 15 shows the pitching moment for maximum positive and negative deflections of the circumferential ones. At AoA < 10 and at 1 m/s; the Anuloid is statically stable for negative vane deflections and unstable for positive vane deflections. For AoA > 10 degrees, the opposite behavior was found; the Anuloid is statically unstable for negative vane deflections and stable for positive vane deflections. A statically unstable aircraft is, in general, not flyable without a stability augmentation system. At a horizontal velocity of 20 m/s (Fig. 15(b)) the situation is the same. By comparing the plots for 1 m/s and 20 m/s an important observation can be made, the effect of the control surfaces reverses for AoA < 30; this means that

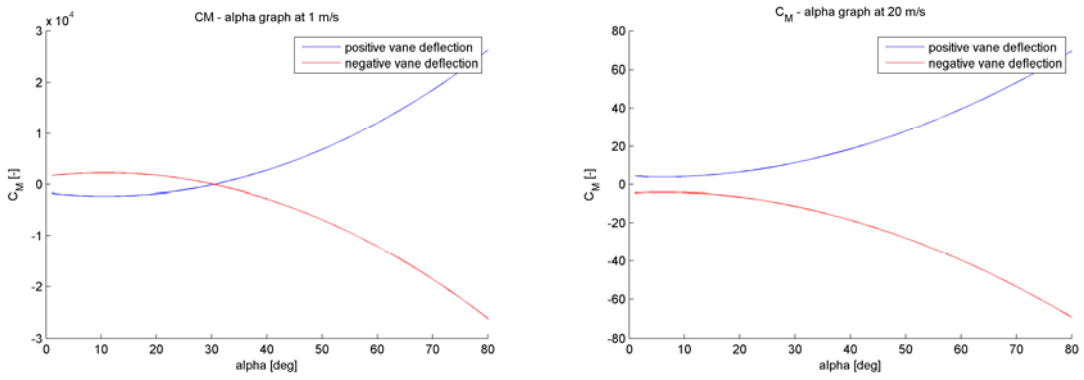

(a) 1 m/s (b) 20 m/s

Fig. 15 Pitching moment coefficient for maximum positive and negative deflections of the pitch control vanes

there is a significant nonlinearity in the dynamics of Anuloid and implies that a nonlinear control system must be used to control the aircraft.

5.3 Dynamic stability analysis

A six degrees of freedom rigid dynamic model of the Anuloid was created for the nonlinear analysis. Six sets of nonlinear partial differential equations were defined which together form the well-known aircraft equations of motion (EOM) (Stevens and Lewis 2003). These equations are the following: the linear dynamics equations, the body angular rate dynamics equations, the Euler angle dynamics equations, the aerodynamic angle dynamics equation and, finally, the navigational dynamics equations. It is important to note that the aircraft EOM are defined in terms of the standard formulation body axis reference frame, where the *X*-axis points forward, the *Y*-axis points to the right and the *Z*-axis points downwards. Also, it is important to note that for the dynamic stability analysis all the dynamic damping coefficients were set to zero. These coefficients are notoriously difficult to determine by either CFD or wind tunnel and in most cases can only be determined during flight testing. For conventional aircraft, established rules of thumb (e.g., the DATCOM) can be used to obtain the initial values for the damping coefficients. The rules of thumb are not applicable however to the Anuloid due to its unconventional configuration and resulting dynamics. By neglecting the dynamic damping, the dynamic stability analysis should be seen as the worst case scenario, the damping coefficients, when present, will always increase the dynamic stability of the aircraft.

The dynamic system representation is

$$\dot{x} = f(x, U) \tag{1}$$

where x is the state vector, U is the input vector, f is the state transition equation and $\dot{x}$ is the state derivative with respect to the time . The state vector is defined as follows

$$x = \begin{bmatrix} u & v & w & p & g & r & \varphi & \theta & \psi & \alpha & \beta & P_N & P_E & h \end{bmatrix} \tag{2}$$

where u, v and w are the velocities (m/s) along the X, Y and Z body axis of the aircraft (note that the Z-axis points downward, see Fig. 9); p, q and r are the body angular rates (rad/s); φ, θ, ψ are the Euler roll, pitch and yaw angles (rad), respectively. The angle of attack is α (rad) and the angle of sideslip is β (rad). Finally P_N, P_E and h, are the North position, the East position and the altitude (m), respectively.

The input vector is

$$U = [a_{da} \quad a_{de} \quad a_{dr} \quad V_f] \tag{3}$$

where a_{da} is the deflection angle of the control vanes that produces a rolling moment, a_{de} is the deflection angle of the control vanes that produces a pitching moment and a_{dr} is the deflection angle of the control vanes resulting in a yawing moment (all in radians). The final control variable is V_f which is the volume flow through the rotor (in m^3/s).

The linear dynamics equations are then given as follows

$$\begin{bmatrix} \dot{u} \\ \dot{v} \\ \dot{w} \end{bmatrix} = \frac{1}{m} \begin{bmatrix} X_T + X_{ae} \\ Y_T + Y_{ae} \\ Z_T + Z_{ae} \end{bmatrix} + \begin{bmatrix} p \\ q \\ r \end{bmatrix} \times \begin{bmatrix} u \\ v \\ w \end{bmatrix} + g \begin{bmatrix} -\sin\theta \\ \cos\theta \sin\varphi \\ \cos\theta \cos\varphi \end{bmatrix} \tag{4}$$

Where $\dot{u}$, $\dot{v}$, $\dot{w}$ are the linear accelerations (m/s^2). The total mass of Anuloid, denoted by 'm', was set equal to 1105 kg. The thrust forces X_T, Y_T, Z_T (N) and the aerodynamic forces X_{ae}, Y_{ae}, Z_{ae} (N) along the body axes were derived from the CFD calculations. The acceleration of gravity is 'g' (9.81 m/s^2).

The rotational dynamics equations are

$$\begin{bmatrix} \dot{p} \\ \dot{q} \\ \dot{r} \end{bmatrix} = J^{-1} \begin{bmatrix} L_T + L_{ae} \\ M_T + M_{ae} \\ N_T + N_{ae} \end{bmatrix} + J^{-1} \left(\begin{bmatrix} p \\ q \\ r \end{bmatrix} \times J \begin{bmatrix} p \\ q \\ r \end{bmatrix} \right) \tag{5}$$

where $\dot{p}$, $\dot{q}$, $\dot{r}$ are the body rotational accelerations (rad/s^2), J is the inertia matrix that was extracted from the CAD model and is equal to

$$J = \begin{bmatrix} 775.77 & 0.57 & 0 \\ 0.57 & 775.79 & 0 \\ 0 & 0 & 1235.05 \end{bmatrix} \tag{6}$$

The thrust moments (L_T, M_T, N_T (Nm)) and the aerodynamic moments (L_{ae}, M_{ae}, N_{ae} (Nm)) were derived from the CFD calculations. The body angular rate dynamics (Euler dynamics) were given as follows

$$\begin{bmatrix} \dot{\varphi} \\ \dot{\theta} \\ \dot{\psi} \end{bmatrix} = \begin{bmatrix} 1 & \sin\varphi\tan\theta & \cos\varphi\tan\theta \\ 0 & \cos\varphi & -\sin\varphi \\ 0 & \dfrac{\sin\varphi}{\cos\theta} & \dfrac{\cos\varphi}{\cos\theta} \end{bmatrix} \begin{bmatrix} p \\ q \\ r \end{bmatrix} \tag{7}$$

where $\dot{\varphi}$, $\dot{\theta}$, $\dot{\psi}$ are the Euler angle rotational accelerations (rad/s^2). The aerodynamic angle derivatives (rad/s^2) are

$$\begin{bmatrix} \dot{\alpha} \\ \dot{\beta} \end{bmatrix} = \begin{bmatrix} \dfrac{u \cdot \dot{w} - w \cdot \dot{u}}{u^2 + w^2} \\ \dfrac{\dot{w} \cdot \sqrt{u^2 + v^2 + w^2} - v \cdot \sqrt{u^2 + v^2 + w^2}}{\sqrt{u^2 + v^2 + w^2}\left(u^2 + w^2\right)} \end{bmatrix} \tag{8}$$

Finally, the navigation position derivatives are given as follows

$$\begin{bmatrix} P_N \\ P_E \\ \dot{h} \end{bmatrix} = \begin{bmatrix} \cos\theta\cos\psi & -\cos\varphi\sin\psi + \sin\varphi\sin\theta\cos\psi & \sin\varphi\sin\psi + \cos\varphi\sin\theta\cos\psi \\ \cos\theta\sin\psi & \cos\varphi\cos\psi + \sin\varphi\sin\theta\sin\psi & -\sin\varphi\cos\psi + \cos\varphi\sin\theta\sin\psi \\ \sin\theta & -\sin\varphi\cos\theta & -\cos\varphi\cos\theta \end{bmatrix} \begin{bmatrix} u \\ v \\ w \end{bmatrix} \tag{9}$$

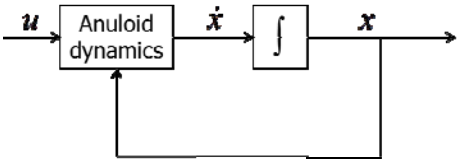

Fig. 16 Block diagram of dynamic simulation

Where $\dot{P}_N$, $\dot{P}_E$ and $\dot{h}$ are the velocities (m/s) in the North direction, the East direction and altitude, respectively. Fig. 16 shows the open-loop simulation where the "Anuloid dynamics" block contains the state transition equations $\dot{x} = f(x, U)$.

First, the dynamic stability during the vertical flight was analyzed (i.e., $U = 0$). For this, the aircraft was first brought into a trimmed condition in the sense that the body accelerations and the angular rates are equal to zero. At the trimmed condition, a step input was given on the radial control vane.

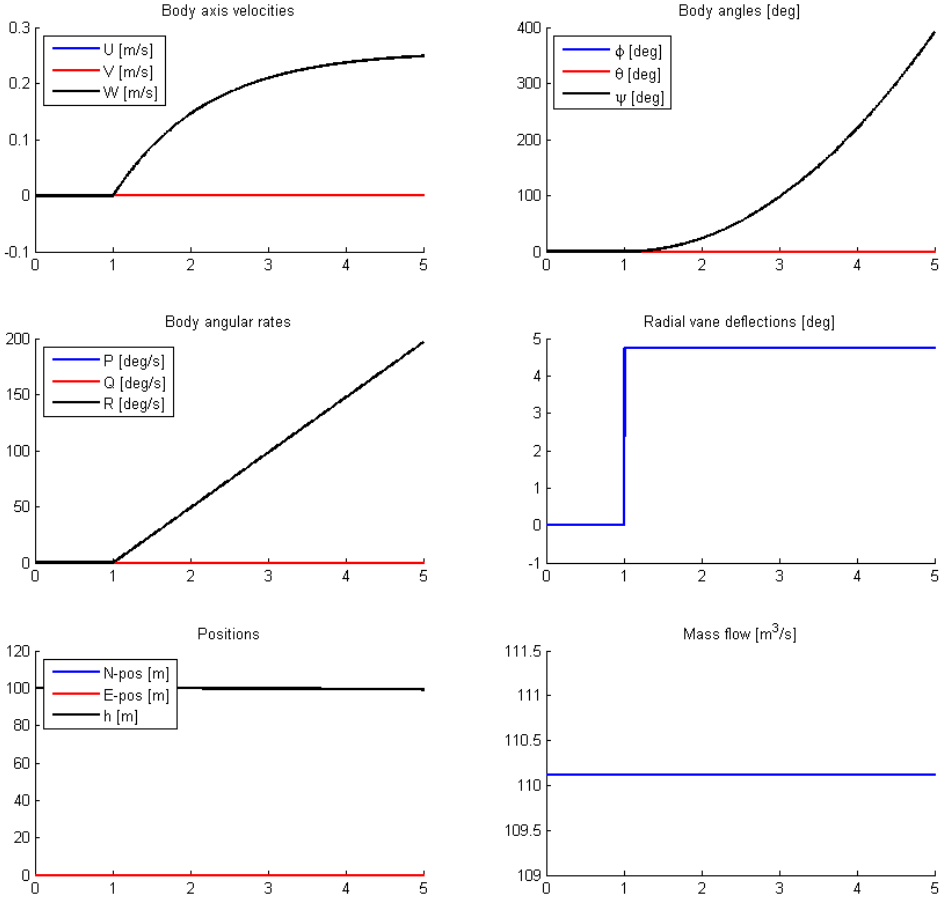

Fig. 17 Step input on the radial control vane response

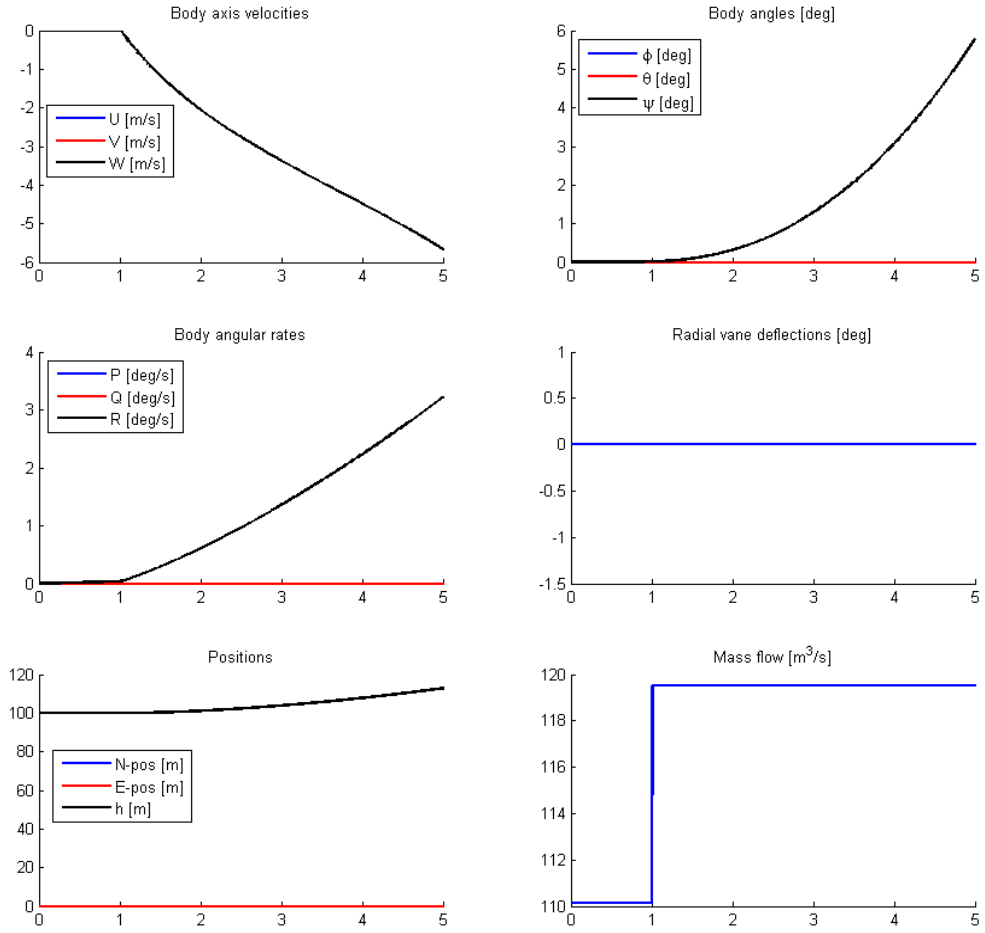

Fig. 18 Step input on the mass flow control parameter response

Fig. 17 shows the responses and it can be seen that the yaw rate increases linearly with the radial vane extension. This is a desirable behavior, any damping coefficients will limit the maximum yaw rate. Then, a step input on the volume flow control parameter was considered and the results are shown in Fig. 18. The ascent velocity increases ($W < 0$) to more than 5 m/s, but the increase is nonlinear. The yaw rate increases due to the torque effect of the main rotor which is not compensated by an extra radial vane deflection. Again, these are desirable properties from the stability point of view.

The dynamic stability during the horizontal flight was investigated by first bringing the aircraft into a semi-trimmed condition in the sense that the body accelerations and the angular rates are close to zero. At this semi-trimmed condition, a pulse input was given on the pitch control vanes. Fig. 19 shows that the pitch rate q suddenly increases in magnitude and keeps increasing even after the vanes have been moved back to the trimmed state. These results show that Anuloid is dynamically unstable during forward flight. The time to double amplitude, which is a measure of instability, is around 2 seconds.

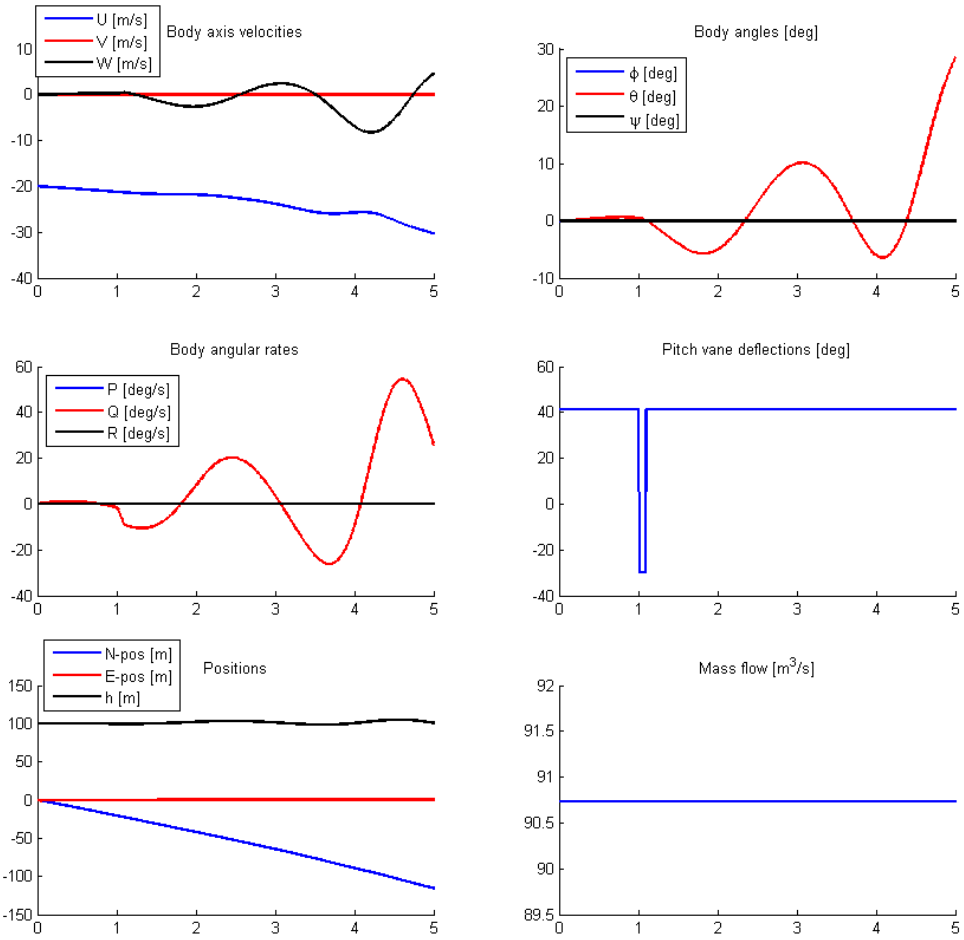

Fig. 19 Pulse input on the pitch control vane response

Next, a pulse input on the mass flow control parameter was given (Fig. 20). Again, the pitch rate departs from the trimmed state and significant instability is now also present in the forward and vertical velocities. Again, the time to double amplitude is 2 seconds.

The final analysis is the determination and classification of the trim points of the Anuloid. In order to find the trim points, a grid with initial trim conditions was defined and a nonlinear optimization algorithm was used to determine the control inputs for which the state derivatives approach zero. Fig. 21 shows the trim points that were found. For the vertical flight (left hand plot) it can be seen that at each velocity and yaw rate a trim point exists and, in most cases, it is stable. For high ascent velocities, the trim points are unstable due to the saturation of the radial control vanes. For the horizontal flight, only unstable trim points can be found. This is an expected result since the Anuloid is unstable during the horizontal flight.

The results from the flyability analysis show that:

(1) The Anuloid can provide sufficient lift and thrust to take off, fly horizontally, and land using the Honeywell T3517 turbine engine.

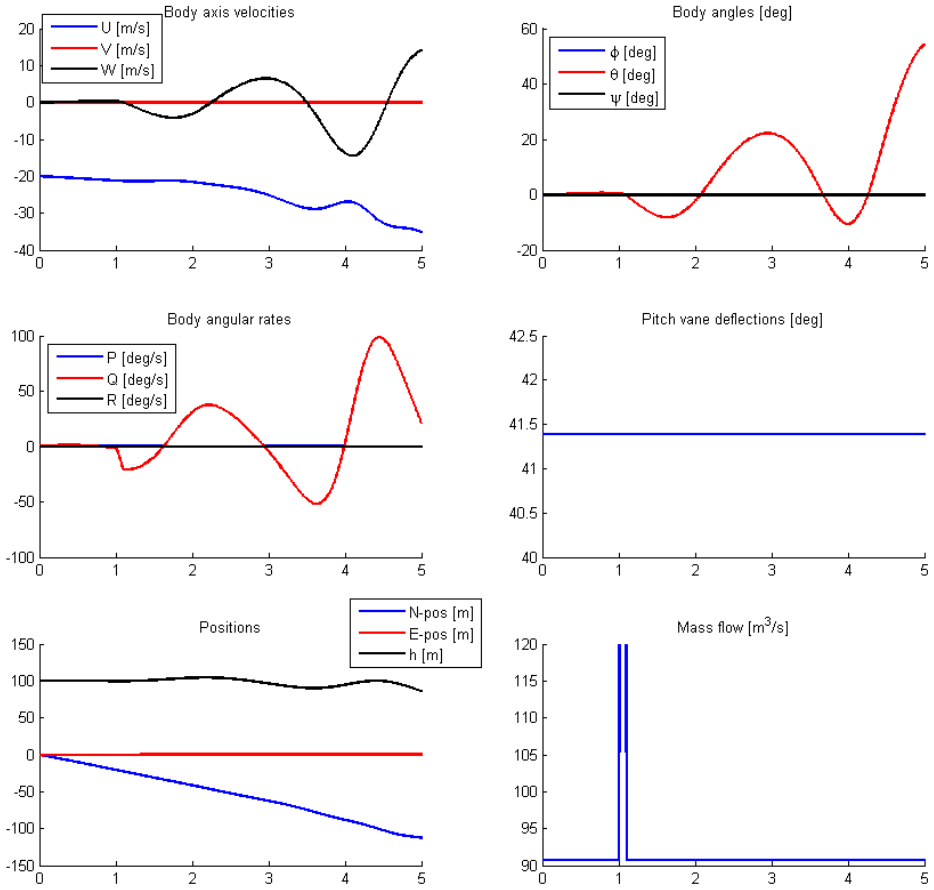

Fig. 20 Pulse input on the mass flow control parameter response

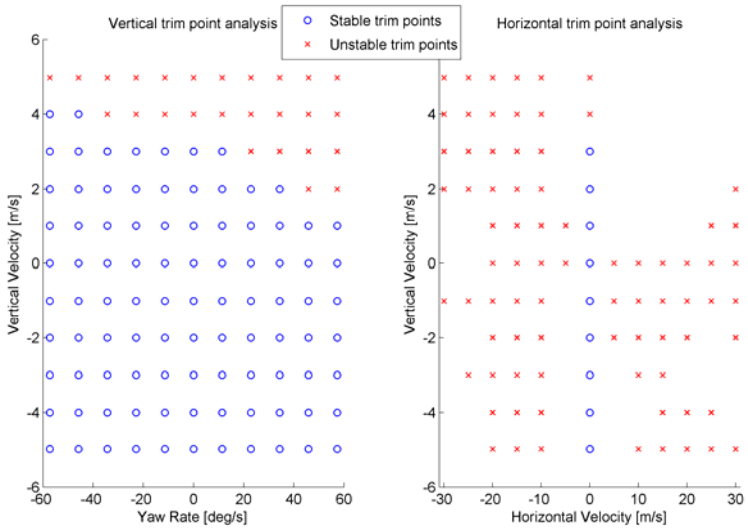

Fig. 21 Trim points

(2) The Anuloid is statically unstable during the horizontal flight and the effect of the pitch control vanes on the pitching moment reverses at an angle of attack of 10 degrees.
(3) The Anuloid has desirable (linear) dynamic responses during vertical flight. Many stable trim points can be found in this flight region, with the only instabilities occurring during the fast ascending flight.
(4) The Anuloid is dynamically unstable during the horizontal flight, with a time to double the amplitude of 2 seconds. While not dramatically unstable, the Anuloid is projected to have inadequate handling qualities during forward flight requiring the use of an automatic control system.

6. Conclusions

This paper has presented the results from the early development of an innovative disk-shaped VTOL aircraft, the Anuloid. This aircraft is thought for emergency operations and civil transportation in urban areas and can be considered as an improved VTOL with respect to helicopters in terms of lowered noise pollution (due to the ducted engine) and wider operational scenarios. The main features of this aircraft are the following: the lift for take-off and cruise is provided by a fan that is powered by a turboshaft and the Coanda effect; the anti-torque is provided by a system of fixed and swiveling radial vanes by controlling the swirl of the flow that outgoes from the engine fan. The flight control is obtained by means of the radial vanes and of the individually swiveled circumferential vanes. The early development focused on the weight estimation, the definition of the structural layout, the CFD and the flyability analysis. The aim of these preliminary activities was the investigation of the main physical capabilities of the aircraft to highlight the critical points to be further investigated in the next phases of the design.

The main conclusions are the following:

- The CFD analyses have highlighted the efficiency of the control vanes and the stability of the Coanda effect upon a minor modification of the internal duct geometry.
- The flyability analysis has shown that the vertical flight of the Anuloid has satisfactory flying qualities and that there is a sufficient lift production.
- The dynamic stability analysis has shown that the Anuloid is dynamically unstable during horizontal flight. While not dramatically unstable, the Anuloid can have inadequate handling qualities during the forward flight.
- Due to the observed instability, the Anuloid requires an automatic flight control system that is capable of stabilizing the aircraft, in particular during horizontal flight.
- The structural analysis has shown that no particular structural issues should arise from the structural design.

Further developments must deal with the experimental analysis of the Coanda effect and of the anti-torque mechanism, the development of an automatic flight control system and a detailed CFD analysis of the internal and external flows and of the transition phases.

Acknowledgments

The research described in this paper was financially supported by the European FP7 project “ANULOID” (ACP2-GA-2013-334861-ANULOID).

References

Angle, G., O'Hara, B., Huebsch, W., Smith, J., Joslin, R.D. and Jones, G.S. (2006), "Experimental and computational investigation into the use of the Coanda effect on the Bell A821201 airfoil", *Progress in Astronautics and Aeronautics*: *Applications of Circulation Control Technology*, **214**, pp. 277-292.

Barlow, C., Lewis, D., Prios, S.D., Odedra, S., Erbil, M.A., Karamanoglou, M. and Collis, R. (2009), "Investigating the use of Coanda effect to create novel unmanned aerial vehicles", *Proceedings of the International Conference on Manufacturing and Engineering Systems*, Huwei, Taiwan, December, pp. 386-391.

Bianco-Mengotti, R. (2012), "The Agusta Westland path to the new-generation tilt-rotor", *CESMA - The future of rotary wing*, Rome.

Crivoi, O., Doroftei, I. and Adascalitei, F. (2013), "A survey of unmanned aerial vehicles based on Coanda effect", *Tehnomus Ji*., **20**, 338-344.

Curtis, P. (2010), "VSTOL integration", *Encyclopedia of Aerospace Engineering*.

Deckert, W. (1995), "The lift-fan aircraft: Lessons learned", *Nasa Contractor Report*, 196694.7.

Federal Aviation Administration (2013), *Noise Certification Standards for Tiltrotors*, pp. 1133-1143.

Fite, E.B. (2013), "Ducted and unducted fans in airbreathing engines", *Encyclopedia of Aerospace Engineering*, 1-14.

Gent, R. (2010), "Ice detection and protection", *Encyclopedia of Aerospace Engineering*.

Hirschberg, M.J., Müller, T. and Rocher, A. (2002), "French high-speed V/STOL concepts of the 20th century", *AIAA Biennial International Powered Lift Conference and Exhibit*, Williamsburg, VA, USA, November.

Hirschberg, M.J., Müller, T. and Piñero, E. (2003), "Italian V/STOL concepts of the 20th century", *American Helicopter Society 59th Annual Forum*.

Janda, Z. (2009), *Aircraft Propeled by Ducted Fan*, Czech patent CZ 303326.

Landis, K.H., Davis, J.M., Dabundo, C. and Keller, J.F. (1994), "Advanced flight control technology achievements at Boeing Helicopters", *Int. J. Control*, **59**(1), 263-290.

Lindenbaum, B. and Blake, W. "The VZ-9 "Avrocar"".
Available at: www.robertcmason.com/textdocs/avro-car-VZ9.pdf

Johnson, W. (2004), *Helicopter Theory*, Dover Publications, New York, NY, USA.

Knowles, K. (2010), "Introduction to aerial vehicle flight mechanics, stability and control", *Encyclopedia of Aerospace Engineering*.

Lindenbaum, B. (1986), "V/STOL concepts and developed aircraft. Volume 1. A historical report (1940-1986)", *Flight Dynamics Laboraory Report*, AFWAL TR 86-3071 Volume 1.

Maisel, M.D., Giulianetti, D.J. and Dugan, C. (2000), *The History of The Xv-15 Tilt Rotor Research Aircraft*: *From Concept to Flight*, The NASA History Series, NASA SP-2000-4517.

Nelms, W.P. and Anderson, S.B. (1984), "V/STOL concepts in the United States: Past, present, and future", *National Aeronautics and Space Administration*, *Ames Research Center*.

Stepniewski, W.Z. and Keys, C.N. (1984), *Rotary-Wing Aerodynamics*, Dover Publications, New York, NY, USA.

Stevens, B.L. and Lewis, F.L. (2003), *Aircraft Control and Simulation*, John Wiley & Sons, Ltd.

Urban Aeronautics, *www.urbanaero.com*

EC